Journal of Catalysis **182,** 430–440 (1999)
Article ID jcat.1998.2333, available online at http://www.idealibrary.com on IDEAL®

# Kinetics of the Selective Low-Temperature Oxidation of CO in $H_2$-Rich Gas over Au/$\alpha$-$Fe_2O_3$

M. J. Kahlich,[1] H. A. Gasteiger,[2] and R. J. Behm

*Abteilung Oberflächenchemie und Katalyse, Universität Ulm, D-89069 Ulm, Germany*

Received July 30, 1998; revised October 26, 1998; accepted November 3, 1998

**The selective CO oxidation (also referred to as PROX) on a Au/$\alpha$-$Fe_2O_3$ catalyst in simulated reformer gas (low concentrations of CO and $O_2$, 75 kPa $H_2$, balance $N_2$) at atmospheric pressure was investigated over almost two orders of magnitude in CO partial pressure (0.025–1.5 kPa) and over a large range of $p_{O_2}/p_{CO}$ ratios (0.25–10). Quantitative evaluation of CO oxidation rates as a function of CO and $O_2$ partial pressure at 80°C yields reaction orders with respect to CO and $O_2$ of 0.55 and 0.27, respectively. The apparent activation energy for this reaction evaluated in the temperature range of 40–100°C is 31 kJ/mol. At 80°C, the selectivity, defined as the ratio of oxygen consumption for CO oxidation to the total oxygen consumption, reaches 75% at large CO partial pressures (1.5 kPa), but decreases significantly with diminishing $p_{CO}$. This is related to the fact that the $H_2$ oxidation rate is independent of the CO partial pressure, consistent with a reaction mechanism where oxygen adsorbed at the metal/metal oxide interface reacts with H and CO adsorbed at low coverages on the supported Au nanoclusters. The selectivity increases with decreasing temperature, reflecting a higher apparent activation energy for $H_2$ oxidation than for CO oxidation. A comparison with Pt/$\gamma$-$Al_2O_3$, a commonly used PROX catalyst with an optimum operating temperature of ca. 200°C, demonstrates that Au/$\alpha$-$Fe_2O_3$ already offers comparable activity and selectivity at 80°C.** 

## 1. INTRODUCTION

Over the last decade, the preferential oxidation of CO (PROX) in $H_2$-rich gas (1) has spurred new interest owing to its application in fuel cell technology, where it may be used to purify $H_2$ produced via steam reforming [e.g., of methanol (2)]. The resulting gas mixture of ideally ~75% $H_2$ and ~25% $CO_2$ is, however, contaminated with at least 1–2% CO (1, 3, 4), which poisons the currently used anode catalysts. To avoid an unacceptable loss of the energy conversion efficiency of the fuel cell, the CO concentration in the reformer gas must be reduced to ≤100 ppm (5).

The selective oxidation of CO is particularly promising for vehicle applications since it allows small-scale operation. Next to reasonably high reaction rates for CO oxidation, the most important requirement of the catalyst is a high selectivity, $S$, with respect to the undesired $H_2$ oxidation side reaction. In this work, $S$ is defined as the ratio of oxygen consumption for CO oxidation to total oxygen consumption (oxygen used for both CO and $H_2$ oxidation). The excess oxygen with respect to the minimum amount of oxygen required for CO oxidation to $CO_2$ in the absence of side reactions is characterized by the process parameter $\lambda$, with $\lambda = 2 \cdot p_{O_2}/p_{CO}$. Therefore, the $\lambda$ value in the PROX process should be as close as possible to one (i.e., stoichiometric) not to oxidize excessive amounts of hydrogen. From the process point of view (reformer, PROX, fuel cell), there are two temperature levels which are particularly convenient for PROX: either the fuel cell operating temperature (80–100°C) or the temperature level of the methanol reformer unit (250–300°C). The commonly proposed PROX catalysts (alumina-supported Pt, Ru, and Rh), however, operate at an intermediate temperature level of 150 to 200°C and significantly lose selectivity at higher temperatures (6–12). For the low temperature level, oxide-supported gold catalysts have been suggested as a promising alternative (13).

Even though pure gold is a poor catalyst for most reactions, due mainly to its weak interaction with most adsorbates and hence limited adsorption capability at 20°C and higher for most gases (14–18), studies by Haruta *et al.* (13, 15, 19–28), Gardner *et al.* (29–31), and other groups (32–38) have shown that highly dispersed gold on metal oxide supports possesses high catalytic activity at low temperatures (<0°C) for CO oxidation. The high activity, which strongly depends on the preparation conditions (15, 23, 36) and catalyst pretreatment (38–40), was generally explained by strong metal support interaction (SMSI) (41). Based on kinetic studies of the CO oxidation reaction on Au supported on $\alpha$-$Fe_2O_3$, $Co_3O_4$, and $TiO_2$ it was proposed that the reaction mechanism involves the reaction of weakly adsorbed CO on Au with oxygen adsorbed at the metal/metal oxide interface (19, 38). For CO oxidation in a $H_2$-rich

[1] To whom correspondence should be addressed. Fax: +49-(731)-50-25452. E-mail: mike.kahlich@chemie.uni-ulm.de.

[2] Current address: Adam Opel AG, Global Alternative Propulsion Center, IPC 81-90, D-65423 Rüsselsheim, Germany.



0021-9517/99 $30.00

gas, however, detailed kinetic studies and, in particular, measurements of the concentration dependence of the selectivity with respect to the undesired $H_2$ oxidation side reaction do not exist.

In the following, kinetic measurements of the selective CO oxidation over Au/$\alpha$-$Fe_2O_3$ in simulated reformer gas (75 kPa $H_2$, 0.025–1.5 kPa CO, balance $N_2$) are presented, both under PROX relevant conditions requiring low $\lambda$ values and at variable excess oxygen ($\lambda = 0.5$–20). The $\alpha$-$Fe_2O_3$ support was chosen because of the very low 50% conversion temperature of the Au/$\alpha$-$Fe_2O_3$ system for CO oxidation ($-70^\circ$C) compared with $\sim 30^\circ$C for $H_2$ oxidation under comparable reaction conditions ($p_{CO}$ or $p_{H_2} = 1$ kPa in air; space velocity: $2 \times 10^4$ Nml $\cdot$ (h $\cdot$ $g_{cat}$)$^{-1}$) (23, 24). We first present data on the CO oxidation rate, the reaction orders, and the partial pressure-dependent selectivity at 80°C. For comparison, the oxidation rate and selectivity were also determined at 40°C. Subsequent temperature-dependent measurements between 40 and 100°C allow determination of the apparent activation energy for both CO and $H_2$ oxidation and yield information on the temperature dependence of the selectivity. In the Discussion, our results are compared with data reported in previous studies on CO oxidation on Au catalysts (Section 4.1), and a quantitative description of the selectivity as a function of CO partial pressure is developed (Section 4.2), followed by a comparison between the reaction characteristics for the present Au catalyst and those for the standard Pt/$\gamma$-$Al_2O_3$ catalyst. Finally, we give an estimate of the performance of the catalysts in a plug-flow PROX reactor.

## 2. EXPERIMENTAL

### 2.1. Catalysts and Reactants

The experiments were performed with 3.15 wt% Au/$\alpha$-$Fe_2O_3$ powder, prepared by coprecipitation. Two aqueous solutions, one containing $HAuCl_4 \cdot 3H_2O$ (Degussa) and $Fe(NO_3)_3 \cdot 9H_2O$ (Fluka) and the other containing sodium carbonate (Fluka), were simultaneously and gradually added into a beaker with distilled water which was vigorously stirred. The reaction mixture was kept at 80°C and special care was taken to maintain the pH of the solution within the range 8.0–8.5 while the two solutions were being added. After filtration, the precipitate was washed with hot water until it was chloride-free (as indicated by reaction with silver nitrate) and dried at 80°C in air (static) for 12 h, followed by calcination in flowing air at 400°C for 2 h. Finally, the catalyst was ground, resulting in an average particle size of ca. 20 $\mu$m. The BET surface area decreased from 250 $m^2$/g obtained after the low-temperature drying step to 55 $m^2$/g for the calcined catalyst. The Au content of the catalyst was determined by atomic absorption spectrometry (AAS). The average gold crystallite size of the calcined catalyst is 6.5 nm (corresponding to a dispersion of ca. 24%) and was obtained from X-ray diffraction line broadening of the Au(111) diffraction peak using the Scherrer equation.

Gases were supplied by Linde AG or Messer Griesheim GmbH. The pure gases [$H_2$ (N5.0), $N_2$ (N5.0, CO-free)] were further purified with gas filter units (Chrompack AG) to remove traces of oxygen, water, and hydrocarbons. The gas mixtures, 2% CO (N4.7) in $H_2$ (N5.6) and 10% $O_2$ (N5.0) in $N_2$ (N5.0, CO-free), were used directly. For calibration, a gas mixture containing 1% $O_2$, 1% CO, 1% $CO_2$, 0.5% $CH_4$, 75% $H_2$, and the remainder $N_2$ was used. The CO-containing gases were stored in aluminum cylinders, and regulators and tubings were of brass or copper to prevent carbonyl formation.

### 2.2. Activity Measurements

Activity measurements were carried out at atmospheric pressure. The reactor consisted of a quartz tube with an inner diameter of 4 mm located in a ceramic tube furnace (catalyst bed 100–120 mg, length $\sim$8 mm). The flow rate of the reaction gas mixture containing variable amounts of CO and $O_2$ as well as 75 kPa $H_2$ (balance $N_2$) was 60 to 135 Nml/min, corresponding to space velocities of $3.0 \times 10^4$ to $8.1 \times 10^4$ Nml (h $\cdot$ $g_{cat}$)$^{-1}$, respectively (all volumetric flow rates are expressed in terms of Nml/min, i.e., ml/min under standard conditions of $1.013 \times 10^5$ Pa and 273.15 K). Since the catalyst bed density is roughly 1 g/$cm^3$, the space velocity range is equivalent to $3.0 \times 10^5$ to $8.1 \times 10^5$ $h^{-1}$. A more detailed description of the reactor system has been reported elsewhere (7).

Reactor inlet and effluent gas streams were analyzed by gas chromatography (80°C, $H_2$ carrier gas) with integrated column switching in combination with two-channel thermal conductivity detection. The detection limit for $CO_2$, $O_2$, $CH_4$, and CO was $\sim$5 volume ppm [for details see Ref. (7)]. CO conversion was calculated from the $CO_2$ signal. It was in good agreement with that calculated from changes in CO concentration, confirming that no side reactions occurred. The errors in the carbon mass balance were always less than 3%. Because of the large error in the quantification of $H_2O$ ($\pm$20%), the selectivity of the CO oxidation reaction ($H_2$ oxidation being the side reaction) was calculated from the oxygen mass balance:

$$S = \frac{0.5 \cdot c^{out}_{CO_2}}{c^{in}_{O_2} - c^{out}_{O_2}} = \frac{0.5 \cdot c^{out}_{CO_2}}{\Delta c_{O_2}}. \qquad [1]$$

Based on experimental scatter, the values of the selectivity evaluated by means of Eq. [1] were correct to within $\pm$3% (absolute). CO oxidation rates, $r_{CO}$, were calculated from the CO conversion and evaluated for the average CO and $O_2$ partial pressure $\bar{p}_i$ in the reactor (arithmetic average) (42). All rates are based on the noble metal weight ($g_{met}$) and expressed in terms of $mol_{CO}$ $g^{-1}_{met}$ $s^{-1}$.

Prior to all experiments, the catalyst was conditioned by calcination in a 10% $O_2/N_2$ mixture at 400°C (30 min, 20 Nml/min) to yield clean surfaces, followed by cooling down to the reaction temperature in pure $N_2$. The gold catalyst was diluted with inert $\alpha$-$Al_2O_3$ (the dilution ratio, $R_{dil}$, denotes the ratio of pure catalyst mass to total mass of the catalyst bed) to keep CO conversions sufficiently small. Considering the strong exothermicity of both the CO and the $H_2$ oxidation reactions ($\Delta H_R$ values of $-566$ kJ/mol$_{O_2}$ and $-482$ kJ/mol$_{O_2}$, respectively), the $O_2$ conversion, $X_{O_2}$, in our measurements was maintained well below 4% for $O_2$ partial pressures between 2.5 and 1 kPa and below 20–30% for $O_2$ partial pressures below 0.1 kPa. This corresponds to a maximum (i.e., at 100% selectivity) adiabatic temperature rise, $\Delta T_{ad,max}$, of <20°C [$\Delta T_{ad,max} \sim 2.0 \cdot X_{O_2} \cdot p_{O_2}$ (in °C), using $X_{O_2}$ (in %) and $p_{O_2}$ (in kPa)] for the highest $O_2$ partial pressure. Therefore, essentially isothermal conditions should be warranted for the small reactor diameter and the typically high catalyst dilutions. For the reaction rates observed in our study [$<10^{-4}$ mol/(cm$^3 \cdot$ s)], mass transport limitations for the ca. 20-$\mu$m particles should be negligible based on the Weisz criterion (42).

In all experiments, we observed a strong initial deactivation of approximately 30% over the first 2 h after the catalyst was put on stream. The deactivation rate slowed down significantly (factor of ~4) in the period between 2 and 10 h on stream, slowly approaching a steady state. This deactivation is similar to what was reported for a kinetic study on CO oxidation on $Au/TiO_2$ (32, 38), where the authors concluded that consistent kinetic data could be acquired approximately 2–3 h after the catalyst was put on stream. Owing to the close similarity between the deactivation behavior of the $Au/TiO_2$ catalyst and that of our catalyst, we have followed the same procedure; kinetic data in our study were acquired at >2 h after the catalyst was put on stream. Modeling of plug-flow reactor performance at high conversion (integral flow) based on our kinetic data and subsequent comparison with experimental results has shown that the acquired kinetic data yield consistent results (43).

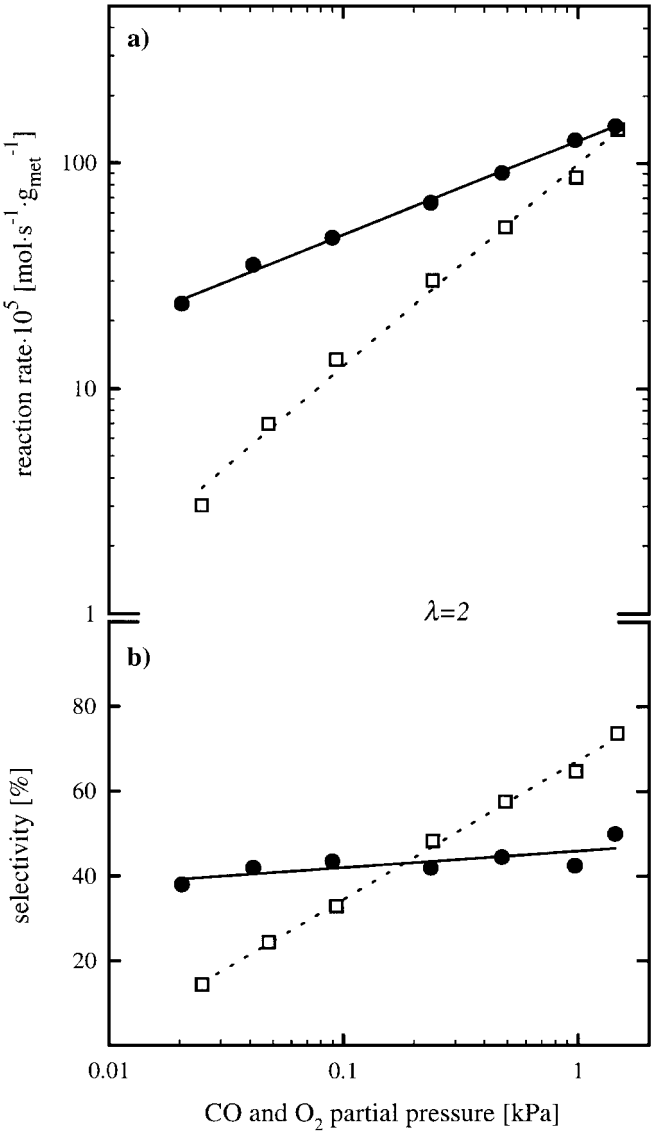


**FIG. 1.** Comparison of (a) reaction rates [mol s$^{-1}$ g$_{met}^{-1}$] and (b) selectivity of 3.15% $Au/Fe_2O_3$ at 80°C (□) with 0.5% $Pt/Al_2O_3$ at 200°C (●), $\lambda = 2$. Least-squares regression lines are fitted to data points. The total weight of the Au catalyst (Pt catalyst) bed was 120 (75) mg; $R_{dil} = 1:25$ (1:9). Simulated reformer gas ($p_{CO} = p_{O_2} = 1.5$–0.02 kPa, 75 kPa $H_2$, balance $N_2$); $\dot{V}_{tot} = 135$ (120) Nml/min.

## 3. RESULTS

### 3.1. Selectivity and Rates at 80°C

In the first set of experiments we investigated the CO partial pressure dependence of the CO oxidation rate in simulated reformer gas (low partial pressures of CO and $O_2$, 75 kPa $H_2$, balance $N_2$). The open squares in Fig. 1a show the CO oxidation rate on $Au/\alpha$-$Fe_2O_3$ at 80°C and $\lambda = 2$ as a function of CO partial pressure. The least-squares regression indicates a CO partial pressure dependence with a slope of $\alpha_{CO}^{\lambda} = 0.85$. Assuming a simple power-law functionality,

$$\log(r_{CO}) = \log(k_{CO}) + \alpha_{CO} \cdot \log(p_{CO}) + \alpha_{O_2} \cdot \log(p_{O_2}), \quad [2]$$

and considering the definition of $\lambda$ ($\lambda = 2 \cdot p_{O_2}/p_{CO}$), the slope of $\log(r_{CO})$ versus $\log(p_{CO})$ at constant $\lambda$ represents the sum of the reaction orders with respect to $p_{CO}$ ($\alpha_{CO}$) and $p_{O_2}$ ($\alpha_{O_2}$) (7):

$$\left(\frac{\partial \log(r_{CO})}{\partial \log(p_{CO})}\right)_{\lambda=\text{const}} = \alpha_{CO} + \alpha_{O_2} \equiv \alpha_{CO}^{\lambda}. \quad [3]$$

The corresponding selectivities are shown in Fig. 1b. The high selectivity of approximately 75% at a CO partial

pressure of 1.5 kPa decreases significantly with CO partial pressure, reaching 15% at a CO partial pressure of ~0.025 kPa. In the definition of selectivity we assumed that it originates from the competition of two parallel reactions, namely, the direct oxidation of both CO ($r_{CO}$) and $H_2$ ($r_{H_2}$):

$$S = \frac{r_{CO}}{r_{CO} + r_{H_2}} = \frac{1}{1 + r_{H_2}/r_{CO}}. \quad [4]$$

If, however, the forward water gas shift reaction (forward-WGS) with product water from $H_2$ oxidation (i.e., $CO + H_2O \rightarrow CO_2 + H_2$) were to occur to any appreciable extent, the observed selectivity would be higher than the selectivity defined by the rates of the direct oxidation reactions (Eq. [4]). Therefore, to determine whether the overall CO oxidation rate is influenced by the forward-WGS, we measured the $CO_2$ formation rate without $O_2$ at 80°C, using a gas composition similar to what was used for the above measurement of the CO oxidation reaction (1 kPa CO, 1.3 kPa $H_2O$, 75 kPa $H_2$, balance $N_2$). The $CO_2$ equilibrium concentration in this mixture is 0.94 kPa at 80°C [based on the equilibrium constant published by Newsome (44)], and for experimental CO conversions of <5%, the $CO_2$ formation rate is unperturbed by equilibrium constraints. Under these conditions, the forward-WGS rate on our 3.15 wt% Au/$\alpha$-$Fe_2O_3$ catalyst is $1.5 \times 10^{-7}$ $mol_{CO}/(g_{Au} \cdot s)$, in good agreement with the rate of $1.7 \times 10^{-7}$ $mol_{CO}/(g_{Au} \cdot s)$ determined by Sakurai *et al.* (45) on their 5 wt% Au/$\alpha$-$Fe_2O_3$ catalyst under similar conditions (1 kPa CO, 2 kPa $H_2O$, balance He; the rate at 80°C was estimated from 100°C data using the quoted activation energy). Compared with these rates, the CO oxidation rates under our experimental conditions are larger by two to four orders of magnitude [$2 \times 10^{-5}$ to $2 \times 10^{-3}$ $mol_{CO}/(g_{Au} \cdot s)$, Fig. 1a], and therefore the contribution of the forward-WGS to the direct CO oxidation rate is negligible.

In principle, it is also conceivable that the formation of water does not proceed via the direct oxidation of $H_2$, but via the reverse water gas shift reaction (reverse-WGS) of $CO_2$ which is formed by CO oxidation. If this were the case, the observed selectivity would be lower than the selectivity toward the direct oxidation reactions of CO and $H_2$. In reverse-WGS measurements over our undiluted 3.15 wt% Au/$\alpha$-$Fe_2O_3$ catalyst at 80°C (1 kPa $CO_2$, 1.3 kPa $H_2O$, balance $H_2$), no CO could be observed even at a low space velocity of $1.61 \times 10^4$ Nml $(h \cdot g_{cat})^{-1}$ [the equilibrium CO concentration in this mixture would be 130 volume-ppm (44)]. At a CO detection limit of 5 volume-ppm, this corresponds to a reverse water gas shift rate of $< 3 \times 10^{-8}$ $mol_{CO}/(g_{Au} \cdot s)$, consistent with the rate of $1 \times 10^{-7}$ $mol_{CO}/(g_{Au} \cdot s)$ measured over 5 wt% Au/$\alpha$-$Fe_2O_3$ at the significantly higher $CO_2$ partial pressure of 23 kPa (67 kPa $H_2$, balance Ar; the rate at 80°C was estimated from 150°C data using the quoted activation energy) (45). Therefore, the $H_2O$ formation rate via the reverse-WGS is several orders of magnitude lower than what is observed during selective CO oxidation, i.e., in the presence of oxygen. In summary, it can be concluded that the measured selectivities in our differential flow experiments are due entirely to the direct simultaneous oxidation of CO and $H_2$ and are not related to either the forward or the reverse water gas shift reaction. The effect of the water gas shift reaction can be observed only at very low space velocities (ca. 100 times lower than in differential flow measurements) in integral flow measurements (43).

### *3.2. Determination of Reaction Orders at 80°C*

In the next series of experiments, $\alpha_{CO}$ and $\alpha_{O_2}$ are determined separately by varying the partial pressure of one of the reactants while keeping the partial pressure of the other constant. The range of $\lambda$ values was roughly one order of magnitude. The reaction rates and resulting selectivities are shown in Fig. 2.

For constant oxygen partial pressure (1 kPa $O_2$), the increase in the reaction rate with $p_{CO}$ corresponds to a reaction order with respect to $p_{CO}$ of 0.58 (open squares, Fig. 2a). The corresponding selectivity (open triangles, Fig. 2b) is a function of the CO partial pressure and decreases considerably from 65% at $p_{CO} = 1$ kPa to 35% at $p_{CO} = 0.1$ kPa. The dependence of $r_{H_2}$ versus $p_{CO}$, which is calculated from the selectivity data in Fig. 2b and Eq. [4], is shown in Fig. 2a (open circles) and demonstrates that the $H_2$ oxidation rate is essentially independent of the CO partial pressure.

When $p_{CO}$ is kept constant (1 kPa CO), the CO oxidation rate exhibits a weak dependence on the oxygen partial pressure, yielding a reaction order with respect to $p_{O_2}$ of 0.23 (Fig. 2c). The selectivity (Fig. 2d) is constant at 65–70% in the entire $p_{O_2}$ range, which implies that the rates of both CO and $H_2$ oxidation have the same dependency on the oxygen partial pressure (see Eq. [4]). This is further discussed in Section 4.2.

From these experiments it can be seen that the reaction order with respect to $p_{CO}$ at constant $\lambda$ ($\alpha^{\lambda}_{CO} = 0.85$, see above) is in good agreement with the sum of $\alpha_{CO} = 0.58$ and $\alpha_{O_2} = 0.23$ (=0.81) determined from the 80°C data in Figs. 2a and 2c (see Eq. [3]), indicating that simple power-law kinetics are sufficient to describe the CO oxidation rate over a rather large $O_2$ and CO partial pressure range. The kinetic parameters determined above were checked by a comprehensive numerical least-squares fit of the 80°C data to Eq. [2], resulting in $k_{CO} = 9.81 \times 10^{-4}$ $mol_{CO}/(g_{Au} \cdot s) \pm 1.6\%$ (for partial pressures in units of kPa), $\alpha_{CO} = 0.55 \pm 5.2\%$, $\alpha_{O_2} = 0.27 \pm 8.8\%$. It should be noted that these simple power-law kinetics merely describe the observed CO oxidation rates at 80°C and do not allow stringent conclusions on the mechanism of the CO oxidation reaction. The latter was attempted in a kinetic and spectroscopic study by Bollinger and Vannice for Au/$TiO_2$ catalysts, where it was concluded that the reaction probably

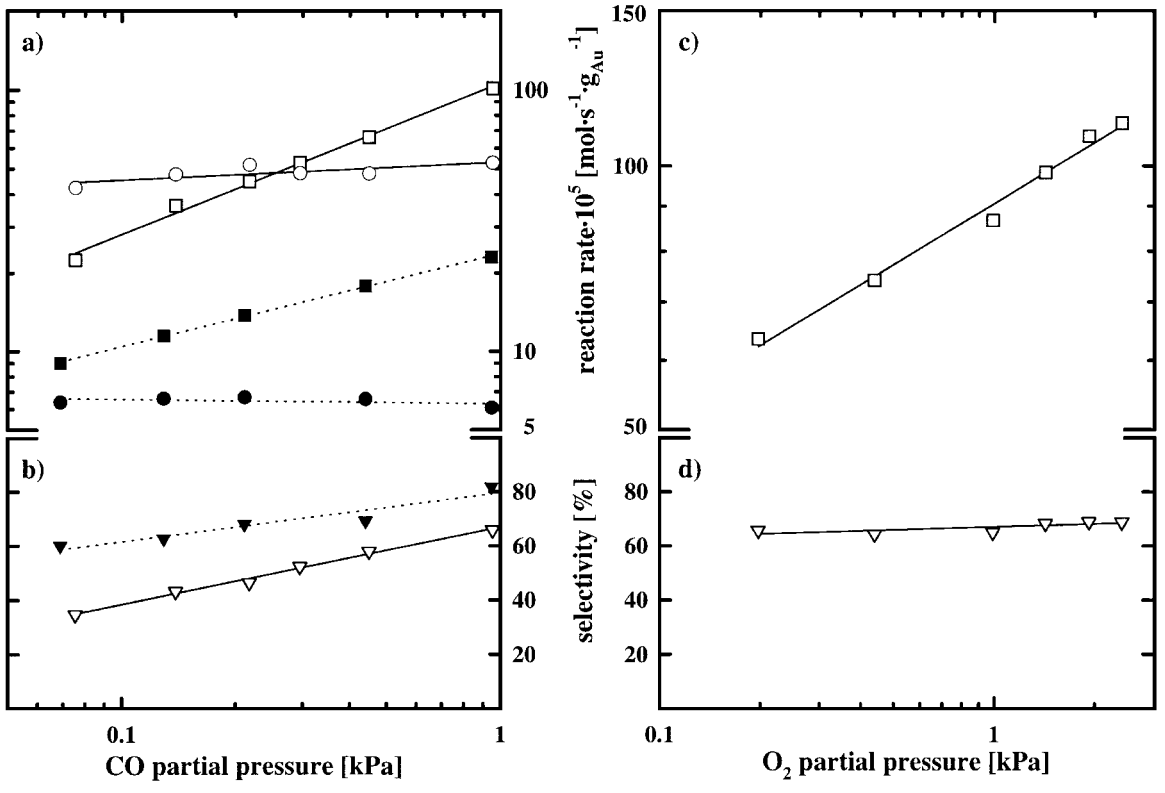


**FIG. 2.** Dependence of reaction rates ($r_{CO}$) [mol $s^{-1}$ $g_{Au}^{-1}$] on (a) $p_{CO}$ (at $p_{O_2} = 1$ kPa) at (□) 80°C and (■) 40°C and (c) $p_{O_2}$ at 80°C (at $p_{CO} =$ 1 kpa) in simulated reformer gas (75 kPa $H_2$, balance $N_2$). (b) and (d) show the corresponding selectivities (▽, 80°C; ▼, 40°C). The total weight of the catalyst bed was 120 mg (80°C)/100 mg (40°C) and 105 mg in the case of $p_{O_2} =$ constant and $p_{CO} =$ constant, respectively. $R_{dil} = 1:6$ (40°C) and 1 : 24 (80°C); $\dot{V}_{tot} = 135(80)$ Nml/min in the case of $p_{O_2} =$ constant ($p_{CO} =$ constant). The circles in (a) refer to the $H_2$ oxidation rate calculated by means of the corresponding selectivities: ○, 80°C; ●, 40°C.

occurs via a noncompetitive Langmuir–Hinshelwood mechanism with nondissociative oxygen adsorption (38). Similar conclusions were drawn in a later study by Cant and Ossipoff (40). The large number of parameters in these more complex models, however, require kinetic data at several different temperatures to attain a statistically significant model selection from several conceivable Langmuir–Hinshelwood models (competitive ↔ noncompetitive, dissociative ↔ nondissociative). Since the focus of our work is to determine whether Au/$\alpha$-$Fe_2O_3$ catalysts are suitable for the PROX process at 80°C, our kinetic measurements were conducted primarily at this temperature, and therefore, we have not attempted to try to fit the observed CO oxidation rates to these more complex models. Nevertheless, within the PROX-relevant $O_2$ and CO partial pressure range, the simple power-law model provides an accurate numerical description of the measured CO oxidation rates.

The significant dependence of the reaction rates on CO and $O_2$ partial pressure derived here for CO oxidation in simulated reformer gas contrasts the findings by Haruta *et al.* (24, 25), who in the absence of $H_2$ under otherwise similar gas compositions ($p_{CO} = 0.2$–6 kPa, $p_{O_2} = 1$–20 kPa) observed that the CO oxidation rate on a 0.66 wt% Au/$\alpha$-$Fe_2O_3$ catalyst at 31°C is essentially independent of the CO and $O_2$ partial pressure, ($\alpha_{CO} = 0, \alpha_{O_2} = 0.05$). This discrepancy may be due either to the influence of $H_2$, to a particle size effect, or to a temperature dependence of the reaction order. The latter was observed for a 2.3 wt% Au/$TiO_2$ catalyst by Lin *et al.* (32), with $\alpha_{CO}$ decreasing from 0.6 to 0.2 as the temperature decreased from 87 to 37°C ($p_{CO} = 1$–25 kPa, $p_{O_2} = 1$–20 kPa, balance He). To examine whether temperature effects play a similar role for our Au/$\alpha$-$Fe_2O_3$ catalyst as for the Au/$TiO_2$ catalyst, which also would account for the difference between Haruta's results and ours, we also investigated the CO oxidation behavior in simulated reformer gas at a lower temperature.

### *3.3. CO Oxidation Rate and Selectivity versus Temperature*

The filled symbols in Figs. 2a and 2b show the variation of the reaction rate and the selectivity as a function of $p_{CO}$ at constant oxygen partial pressure (1 kPa $O_2$) at 40°C in simulated reformer gas (75 kPa $H_2$, balance $N_2$). The reaction order with respect to $p_{CO}$ is 0.35, which is in accordance with the above assumption that $\alpha_{CO}$ diminishes with

temperature (0.55 at 80°C) and is in good qualitative agreement with the above-described data of Lin *et al.* (32) for CO oxidation on Au/$TiO_2$ as well as with later studies on similar Au/$TiO_2$ catalysts (38, 40). Analogous to the 80°C data (open circles in Fig. 2a), the $H_2$ oxidation rate (filled circles in Fig. 2a) is again independent of CO partial pressure. At any CO partial pressure, selectivity is considerably higher at 40°C than at 80°C. This is due to the significant decrease in the $H_2$ oxidation rate by almost one order of magnitude (filled/empty circles in Fig. 2a), whereas the CO oxidation rate decreases by a factor of only ~3–4 depending on the CO partial pressure. Since $r_{CO}$ decreases less strongly with $p_{CO}$ at 40°C than at 80°C, the loss of selectivity with decreasing $p_{CO}$ is less pronounced at low temperatures. Therefore, the difference in selectivity between 40 and 80°C is small (~15%) at high $p_{CO}$ and large (~25%) at low $p_{CO}$ (see Fig. 2b).

To determine the apparent activation energy, $E_A$, the reaction rates at constant gas composition ($p_{CO} = p_{O_2} =$ 1 kPa, 75% $H_2$, balance $N_2$) were measured over the temperature range 40–100°C. The Arrhenius plot of CO oxidation rate in Fig. 3a (open squares) yields an apparent activation energy of 31 kJ/mol, which is relatively small compared with the values obtained on supported Pt catalysts (71 kJ/mol) (7). Under the same conditions, $H_2$ oxidation rates (filled circles in Fig. 3a) yield an apparent activation energy of 50 kJ/mol, accounting for the observed decrease in selectivity with increasing temperature from more than 80% at 40°C to ~60% at 100°C (see Fig. 3b). Qualitatively, this is consistent with a previous report that showed that the temperature required for an appreciable conversion over a Au/$\alpha$-$Fe_2O_3$ catalyst is much higher for $H_2$ oxidation than for CO oxidation (at $p_{CO} = p_{H_2} = 1$ kPa in air) (24).

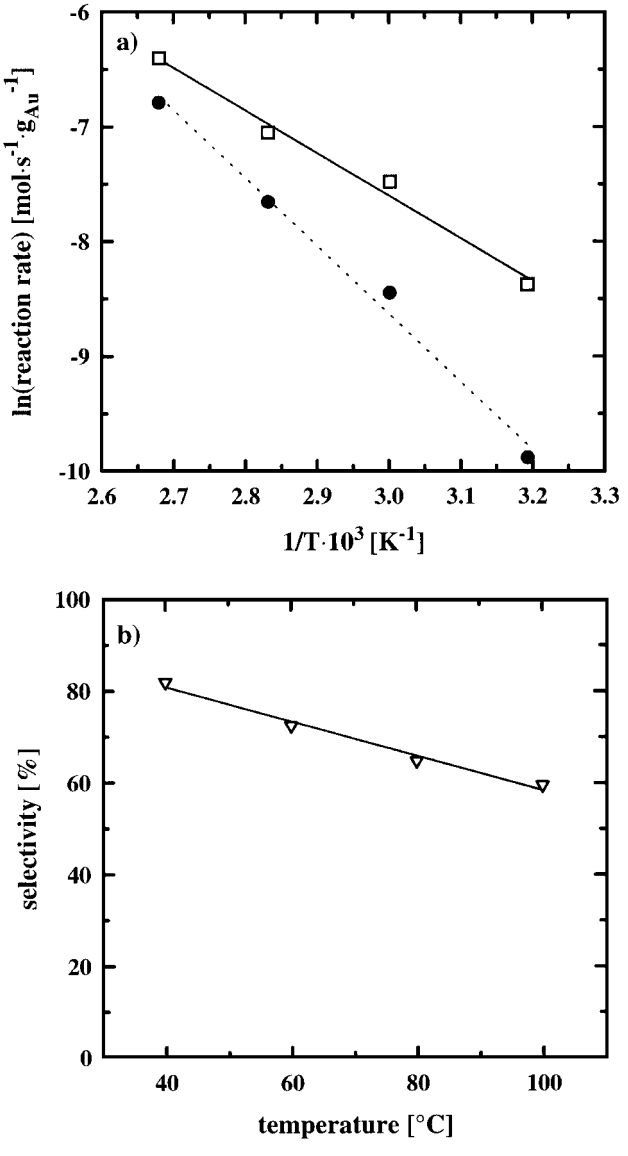


**FIG. 3.** (a) Arrhenius diagram of ln($r$) versus 1/$T$ for CO (□) and $H_2$ (●) oxidation and (b) dependence of the selectivity on reaction temperature at $\lambda = 2$ in simulated reformer gas (1 kPa CO, 1 kPa $O_2$, 75 kPa $H_2$, balance $N_2$). The total weight of the catalyst bed was 100 mg at 40°C and 120 mg at higher temperatures; $R_{dil}$ at 40°C = 1 : 6 and was doubled for every increase in temperature of 20°C; $\dot{V}_{tot} = 135$ Nml/min.

## 4. DISCUSSION

In this article our data are first compared with published rates for CO oxidation in the absence of $H_2$ on different Au/$Fe_2O_3$ catalysts. Subsequently, its potential for application as PROX catalyst is discussed, particularly considering the technical advantages of operating the PROX process at the fuel cell temperature level (~80°C). This includes a quantitative description of the selectivity for CO oxidation as a function of CO and $O_2$ partial pressures (Section 4.2), a comparison of the PROX reaction characteristics over Au/$\alpha$-$Fe_2O_3$ and Pt/$\gamma$-$Al_2O_3$ catalysts (Section 4.3), and an evaluation of the performance of the Au/$\alpha$-$Fe_2O_3$ catalyst at near 100% CO conversion (integral flow), using the kinetic data obtained from the differential flow measurements presented above. This is outlined in Section 4.4, but a more detailed understanding of how the selectivity of the Au/$\alpha$-$Fe_2O_3$ catalyst depends on CO and $O_2$ partial pressures is required.

### *4.1. Comparison with Published CO Oxidation Rates on Au-Based Catalysts*

Published rates for CO oxidation in the absence of $H_2$ (i.e., in inert gas or air) on different Au/$Fe_2O_3$ catalysts at 30°C are summarized in Table 1 in terms of mass-specific reaction rates [$mol_{CO}/(g_{cat} \cdot s)$ and $mol_{CO}/(g_{Au} \cdot s)$] and turnover frequencies (TOFs). As a comparison, the CO oxidation rates on our 3.15 wt% Au/$\alpha$-$Fe_2O_3$ catalyst in the presence of $H_2$ (and reaction water) are given in the first two lines of Table 1 [extrapolated to 30°C using an activation energy of 31 kJ/mol; to estimate the rate for

**TABLE 1**

**Comparison of Published Literature Data for CO Oxidation Rates in the Absence of $H_2$ on $Fe_2O_3$-Supported Gold Catalysts as well as Gold Sponge with Data Obtained in This Work Extrapolated to 30°C (in the Presence of $H_2$)**

| System | Loading (wt%) | Preparation | Particle size (nm) | $p_{CO}$ (kPa) | $p_{O_2}$ (kPa) | $E_A$ (kJ/mol) | $r_{CO}$ at 30°C [mol $(s \cdot g_{cat})^{-1}$] | $r_{CO}$ at 30°C [mol $(s \cdot g_{Au})^{-1}$] | $r_{CO}$ at 30°C [TOF $\times 10^3$] | Ref. |
|---|---|---|---|---|---|---|---|---|---|---|
| Au/$\alpha$-$Fe_2O_3$ | 3.15 | Coprecipitation | 6.5 | 1 | 1 | 31 | $5.1 \times 10^{-6}$ | $1.6 \times 10^{-4}$ | 130 | This work |
| | | | | 1 | 20 | | $1.1 \times 10^{-5}$ | $3.6 \times 10^{-4}$ | 300[a] | This work |
| Au/$Fe_2O_3$ | 3.8 | Coprecipitation | — | 3 | 20 | — | $4.6–9.8 \times 10^{-6}$ | $1.2–2.6 \times 10^{-4}$ | —[b,c] | (39) |
| Au/$\alpha$-$Fe_2O_3$ | 0.66 | Coprecipitation | $3.6 \pm 1.6$ | 0.2–6 | 1–20 | 35 | $1.2 \times 10^{-6}$ | $1.8 \times 10^{-4}$ | 86[d,e] | (24) |
| Au/$\alpha$-$Fe_2O_3$ | 11.5 | Coprecipitation | $4.1 \pm 1.4$ | 1 | 20 | 35 | $>5.7 \times 10^{-6}$ | $>0.5 \times 10^{-4}$ | >27[e,f] | (22, 24) |
| Au/$\alpha$-$Fe_2O_3$ | 5 | Impregnation | 16 | 1 | 20 | 25 | $9.8 \times 10^{-8}$ | $2.0 \times 10^{-6}$ | 3.7[e] | (22) |
| Au/$\alpha$-$Fe_2O_3$ | 3 | Impregnation[g] | >12 | 1 | 20 | 9 | $2.6 \times 10^{-7}$ | $8.6 \times 10^{-6}$ | >12[e] | (36) |
| Au/$\alpha$-$Fe_2O_3$ | 3 | Impregnation[h] | — | 1 | 20 | 21 | $4.2 \times 10^{-8}$ | $1.4 \times 10^{-6}$ | —[e] | (36) |
| Au/Fe$(OH)_3$ | 3 | Impregnation[g] | 2.9 | 1 | 20 | 15 | $1.5 \times 10^{-5}$ | $4.9 \times 10^{-4}$ | 200[e,f] | (37) |
| Au/Fe$(OH)_3$ | 3 | Impregnation[h] | <3.0 | 1 | 20 | 15 | $3.2 \times 10^{-6}$ | $1.1 \times 10^{-4}$ | <45[e] | (37) |
| Au sponge | — | — | — | 5 | 5 | 2.1 | $5.1 \times 10^{-7}$ | $5.1 \times 10^{-7}$ | — | (57) |

[a] Assuming the same oxygen reaction order at 30°C as measured at 80°C (i.e., 0.27).
[b] Depending on catalyst pretreatment.
[c] Initial activity measured during temperature ramp (ramp not specified).
[d] The reaction rate is independent of CO and oxygen partial pressure (reported reaction orders were zero).
[e] No information on after what time conversions were given.
[f] Calculated at high conversion.
[g] Impregnation with a phosphine-stabilized Au complex.
[h] Impregnation with a phosphine-stabilized Au cluster.

$p_{O_2} = 20$ kPa we assumed a temperature-independent $O_2$ reaction order as was closely observed for Au/$TiO_2$ (32)]. The CO oxidation rates referenced to the gold mass for the coprecipitated catalysts (22, 24, 39) range from 0.5 to $2.6 \times 10^{-4}$ $mol_{CO}/(g_{Au} \cdot s)$ and the activity of our gold catalyst compares favorably with these rates and exhibits a very similar activation energy. It should be noted that the activity of our Au/$\alpha$-$Fe_2O_3$ catalyst does not seem to suffer from the presence of water which is formed to significant amounts during the reaction (ca. 0.05 kPa), and according to the data of Haruta *et al.* (26), the CO oxidation rate over Au/$\alpha$-$Fe_2O_3$ might even be enhanced by water vapor [the opposite effect was reported, however, for Au/$TiO_2$ catalysts, which strongly deactivate in the presence of water vapor (38)]. Compared with coprecipitated catalysts, Au/$\alpha$-$Fe_2O_3$ catalysts made by impregnation of $\alpha$-$Fe_2O_3$ support material are one to two orders of magnitude less active (22, 36), consistent with the typically larger Au particle size attained by this preparation method as was discussed by Haruta (19) [reaction rates increase with the inverse second power of the particle diameter (25)]. Recently, however, Yuan *et al.* (37) succeeded in preparing highly active CO oxidation catalysts by impregnating freshly precipitated Fe$(OH)_3$ with phosphine-stabilized Au complexes/clusters, yielding mass-specific CO oxidation rates and turnover frequencies similar to those of highly active coprecipitated catalysts (Table 1). In contrast to the Au/$Fe_2O_3$ catalysts, the mass-specific activity of Au sponge is very low (last line in Table 1), pointing toward the importance of the interaction between Au and the support oxide for CO oxidation activity.

According to an earlier study on the low-temperature (0°C) CO oxidation activity of Au/$Fe_2O_3$, Au/$Co_3O_4$, and Au/$TiO_2$ catalysts, the $TiO_2$ support seemed to result in the highest CO oxidation rates when samples with equal Au particle diameters were compared (24). For the oxidation of 1 kPa CO in air at 30°C, the most active $TiO_2$-based gold catalysts synthesized by the Haruta research group yielded turnover frequencies of 0.12 to 0.26 $s^{-1}$ (3.1–$6.5 \times 10^{-4}$ $mol_{CO}/(g_{Au} \cdot s)$) (19), essentially identical to the activity of our Au/$\alpha$-$Fe_2O_3$ catalyst (Table 1). A similar activity was reported by the Vannice research group for their most active Au/$TiO_2$ catalyst, with a turnover frequency of 0.43 $s^{-1}$ [$6.5 \times 10^{-4}$ $mol_{CO}/(g_{Au} \cdot s)$] under the same conditions (38).

In summary, it may be concluded that the CO oxidation activity (mass-specific reaction rates and turnover frequencies) of our Au/$\alpha$-$Fe_2O_3$ catalyst in $H_2$-rich gas compares quite favorably with the activities of the most active Au/$Fe_2O_3$ and Au/$TiO_2$ catalysts whose reaction rates for the oxidation of pure CO are published in the literature. Furthermore, for our Au/$\alpha$-$Fe_2O_3$ catalyst there seems to be no retardation of the activity by the presence of $H_2O$ vapor [contrary to what was reported for Au/$TiO_2$ (38)], making it a potentially interesting catalyst material for the PROX process.

### 4.2. Selectivity

At constant $p_{CO}$ (Figs. 2c and 2d) we observed a constant selectivity over the entire $p_{O_2}$ range, indicating that the reaction order with respect to $p_{O_2}$ is the same for both CO and $H_2$ oxidation. Furthermore, $r_{H_2}$ was found to be completely decoupled from $r_{CO}$ (Fig. 2a) and it was also shown that the forward and reverse water gas shift reactions are negligible compared with the direct oxidation rates of either CO or $H_2$. Under these conditions and assuming that the rate of $H_2$ oxidation follows a power law analogous to Eq. [2], Eq. [4] may be rewritten as

$$S = \frac{1}{1 + k' \cdot p_{CO}^{-\alpha_{CO}}}, \quad k' = \frac{k_{H_2} \cdot p_{p_{H_2}}^{\gamma}}{k_{CO}}. \qquad [5]$$

Here, $k_{CO}$ and $k_{H_2}$ are the temperature-dependent apparent rate constants for CO and $H_2$ oxidation, respectively, $p_{H_2}$ is the hydrogen partial pressure, and $\gamma$ is the reaction order for $H_2$ oxidation with respect to $p_{H_2}$. At constant temperature and constant hydrogen partial pressure (75 kPa in our study), $k'$ should be independent of $p_{O_2}$ and $p_{CO}$. Since $\alpha_{CO}$ has already been determined (0.55), it must be possible to quantitatively describe the selectivities at 80°C as a function of CO partial pressure using Eq. [5] with $k'$ as the only fitting parameter. This is shown for the data in Figs. 1b and 2b, covering a wide range of $\lambda$ values ($\lambda = 2$–20) and CO partial pressures. As can be seen from Fig. 4 (the dotted curve refers to the numerical fit to Eq. [5]), we obtained excellent agreement with the measured selectivity data. This confirms the above hypothesis that the rates for CO and $H_2$ oxidation on Au/$\alpha$-$Fe_2O_3$ are completely decoupled and hence the selectivity depends on $p_{CO}$, contrary to what is observed for Pt/$\gamma$-$Al_2O_3$ where the selectivity is independent of $p_{CO}$ and $r_{CO}$ at temperatures below 250°C and CO partial pressures ranging from 1.5 to 0.025 kPa (7). Equation [5] also serves as a useful means for the inter- and extrapolation of the selectivity at 80°C, which is a prerequisite for the reactor design calculations below.

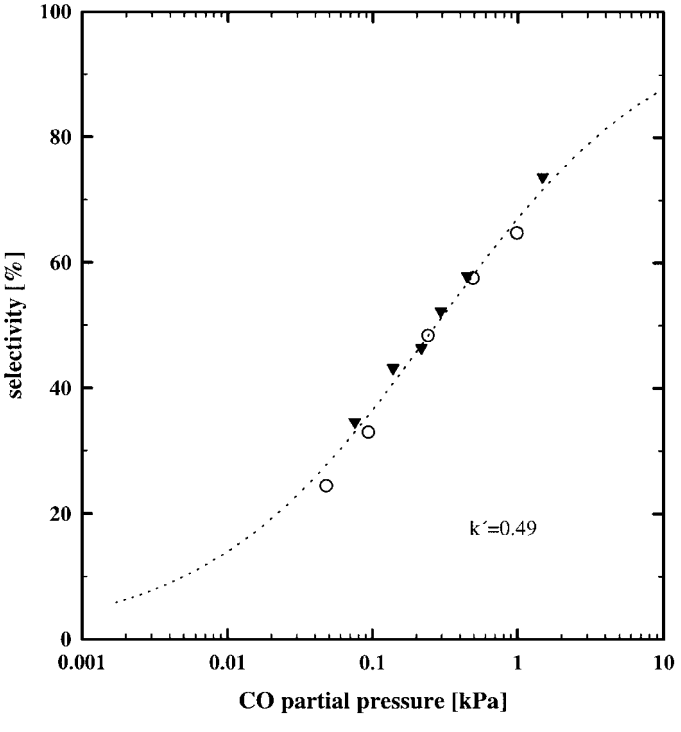


**FIG. 4.** CO concentration dependence of the selectivity at $\lambda = 2$, 80°C (○) and $p_{O_2}$ = constant, 80°C (▼) in simulated reformer gas (75 kPa $H_2$, balance $N_2$). The dotted line is a fit of the selectivity to Eq. [5], with fixed $\alpha_{CO} = 0.55$ and with $k'$ being the only fitting parameter.

### 4.3. Au/$\alpha$-$Fe_2O_3$ versus Pt/$\gamma$-$Al_2O_3$ as PROX Catalyst

We now compare the Au/$\alpha$-$Fe_2O_3$ catalyst at 80°C with a Pt/$\gamma$-$Al_2O_3$ catalyst at its optimum operating temperature of ~200°C for this process, where high CO oxidation rates are still accompanied by high selectivity (7). A quantitative comparison of the reaction rates on the basis of noble metal weight and selectivity of both catalysts at $\lambda = 2$ is given in Fig. 1. Quite clearly, the noble metal-based activity of Au/$\alpha$-$Fe_2O_3$ at 80°C is similar to that of Pt/$\gamma$-$Al_2O_3$ at the much higher temperature of 200°C, particularly at high CO partial pressures (>1.3 kPa), where it is essentially identical in terms of noble metal mass (Fig. 1a). At the lowest CO partial pressure investigated in our study (0.02 kPa), the activities of these catalysts differ by about half an order of magnitude (Fig. 1a). In terms of the reaction kinetics, the two catalysts differ primarily in their partial pressure dependence, in their apparent activation energy (kinetic parameters are summarized in Table 2), as well as in their selectivity behavior as a function of $p_{CO}$ (Fig. 1b).

In a recent study (7) we found that the selectivity between 150 and 200°C on Pt/$\gamma$-$Al_2O_3$ is approximately 40% and is essentially independent of $p_{CO}$ and $\lambda$ over a wide range of CO partial pressures (0.02–1.5 kPa) and two orders of magnitude in reaction rates. This implies (see Eq. [4]) that $r_{CO}$ and $r_{H_2}$ must be directly proportional and must remain at a constant ratio of ~1.5. Furthermore, the steady-state CO coverage, under reaction conditions, was found to be very high (46, 47); hence $H_{ad}$ and $CO_{ad}$ are coadsorbed on the platinum surface at close to CO saturation coverage, thus limiting the dissociative adsorption of oxygen. This situation is characteristic of the so-called low-rate branch for CO oxidation (48), and one would expect a positive reaction order with respect to $p_{O_2}$ and a negative one with respect to $p_{CO}$ (48, 49), consistent with our kinetic measurements (see Table 2). In this reaction regime, the rate-determining step for the oxidation of both CO and coadsorbed hydrogen would be the dissociative adsorption of oxygen in a nearly saturated CO adlayer, effecting the observed coupling of $r_{CO}$ and $r_{H_2}$. The presence of a nearly saturated CO adlayer under reaction conditions is consistent with

**TABLE 2**

**Power-Law Rate Constants ($k_{CO}$), Reaction Orders ($\alpha_{CO}$, $\alpha_{O_2}$), and Activation Energies ($E_A$) for 3.15 wt% Au/$\alpha$-$Fe_2O_3$ at 80°C and for 0.5 wt% Pt/$\gamma$-$Al_2O_3$ at 200°C[a]**

| System | $k_{CO}$ ($mol_{CO}/(g_{met} \cdot s)$) | $\alpha_{CO}$ | $\alpha_{O_2}$ | $E_A$ (kJ/mol) | Ref. |
|---|---|---|---|---|---|
| Au/$\alpha$-$Fe_2O_3$ at 80°C | $9.81 \times 10^{-4}$ | $0.55 \pm 0.03$ | $0.27 \pm 0.02$ | 31 | This work |
| Pt/$\gamma$-$Al_2O_3$ at 200°C | $13.8 \times 10^{-4}$ | $-0.42 \pm 0.05$ | $0.82 \pm 0.05$ | 71 | (7) |

[a] Rate constants and reaction orders as defined in Eq. [2] for partial pressures in units of kPa.

the high CO adsorption energy on platinum surfaces, with low-coverage values ranging from 115 kJ/mol for the reconstructed Pt(100) surface (50) to 134 kJ/mol for Pt(111) (51) and a maximum of 183 kJ/mol for Pt(110) (52).

Contrary to the high CO adsorption energies on platinum, the values reported for the low-coverage CO adsorption energies on gold surfaces are much smaller, ranging from 58 kJ/mol for the reconstructed Au(100) surface (53) and 55 kJ/mol for polycrystalline Au films (54) as well as Au(332) (55) to values below 33 kJ/mol for Au(110) (16). Consistent with these low CO adsorption energies, a strong decrease in the CO coverage with decreasing CO partial pressure (from 1 to 0.03 kPa) was observed in FTIR measurements on $TiO_2$-supported Au nanoparticles at room temperature (56). Therefore, it is reasonable to assume that the CO coverage on the Au particles of our Au/$\alpha$-$Fe_2O_3$ catalyst under reaction conditions (40–80°C and $p_{CO} = 1.5$–0.02 kPa) is very low. While the reaction between atomically adsorbed oxygen and adsorbed carbon monoxide was shown to occur readily on Au(110) under ultrahigh vacuum conditions and temperatures between 273 and 400 K (16), the dissociative adsorption of oxygen on the clean Au(110) surface is strongly kinetically inhibited (17). This explains the low activity of unsupported Au particles for the oxidation of CO with $O_2$ (e.g., Au sponge, see Table 1) and supports the reaction mechanism for CO oxidation over Au/$TiO_2$ catalysts outlined by Bollinger and Vannice (38), where CO adsorbed on Au nanoparticles reacts with oxygen activated at the gold/metal oxide interface via a noncompetitive Langmuir–Hinshelwood mechanism. Using the CO equilibrium adsorption constant derived from their numerical fit of their measured CO oxidation kinetics, one would predict a very low CO coverage of 0–0.13 for the highest CO partial pressure of 1.5 kPa used in our study at temperatures as low as 30°C. This is consistent with the above-mentioned CO adsorption energy ranging from 58 to 33 kJ/mol. If one assumes that the CO coverage is not saturated under reaction conditions, the noncompetitive Langmuir–Hinshelwood mechanism proposed by Bollinger and Vannice (38) as well as by Haruta (15) is at least qualitatively consistent with the observed increase in CO reaction order with temperature. It should, however, be mentioned that these low CO coverages in our experiments would predict a CO reaction order of nearly one ($\alpha_{CO} = 1 - \theta_{CO}$) for a simple Langmuir–Hinshelwood mechanism, contrary to our numerical results using simple power-law kinetics over almost two orders of magnitude of CO partial pressure. This may be reconciled by considering that the overall reaction sequence most likely also involves other reaction steps like the surface diffusion of CO (adsorbed on the Au particle) to the Au/metal oxide interface, where the reaction takes place and where the local CO coverage might be much larger. Therefore, the above-mentioned simple noncompetitive Langmuir–Hinshelwood mechanism which assumes a homogenous distribution of the reactant over the entire surface of the gold particle can be only a very approximate description of the kinetics.

Similar to $O_2$ adsorption, the dissociative adsorption of hydrogen is very weak on Au surfaces (14, 17), although a finite $H_2$ oxidation rate can be observed over Au(110) in the presence of atomically adsorbed oxygen (17). Therefore, both CO coverage and H coverage of the Au nanoparticles are probably very low under our reaction conditions, so that the oxidation of CO does not interfere with the oxidation of coadsorbed hydrogen, explaining the observed independence of $r_{CO}$ and $r_{H_2}$ (Fig. 2a).

### *4.4. Process Parameter for Application in a Plug-Flow PROX Reactor*

To examine the implications of the reaction behavior of Au/$\alpha$-$Fe_2O_3$ for application in the PROX process and to compare it with the Pt/$\gamma$-$Al_2O_3$ catalyst we now determine the $\lambda$ value and the noble metal mass required for 99% conversion of 1.5 kPa CO in simulated reformer gas (variable $O_2$ partial pressure, 75 kPa $H_2$, balance $N_2$) in a plug-flow PROX reactor. This is done by using the concentration dependence of the selectivity (Eq. [5]) and by numerically integrating over the volume elements ($dV$) of a plug-flow reactor. The rate equation for the selective CO oxidation either over Au/$\alpha$-$Fe_2O_3$ at 80°C or over Pt/$\gamma$-$Al_2O_3$ at 200°C (see Table 2) was used to calculate the entering and exiting CO concentrations and $r_{CO}$ in every $dV$, which was then integrated over the reactor volume using the plug-flow reactor equation (42). This allows determination of the minimum $\lambda$ value, $\lambda_{min}$, and the required mass of noble metal,

$m_{met}$, for a specific throughput per liter of reformer gas per minute (evaluated at standard conditions of 273.15 K and $1.013 \times 10^5$ Pa). The results for the two catalysts are [for details see Ref. (43)]:

$$\text{Au}/\alpha\text{-Fe}_2\text{O}_3\ (80^\circ\text{C}): \quad \lambda_{min} = 1.8, \quad m_{Au} = 23 \cdot \text{mg/(Nliter/min)},$$

$$\text{Pt}/\gamma\text{-Al}_2\text{O}_3\ (200^\circ\text{C}): \quad \lambda_{min} = 2.2, \quad m_{Pt} = 9.8 \cdot \text{mg/(Nliter/min)}.$$

As can be seen, the gold catalyst enables the use of a considerably lower $\lambda$ value but the mass of noble metal is higher by a factor of approximately 2.5. The lower $\lambda_{min}$ is due to the initially very high selectivity at high $p_{CO}$ on Au/$\alpha$-$Fe_2O_3$; the requirement of a higher noble metal mass in the case of the gold catalyst stems mainly from the higher reaction rates at low $p_{CO}$ on Pt/$\gamma$-$Al_2O_3$ (see Fig. 1). The validity of these calculations was confirmed in isothermal integral flow experiments (43). These measurements also revealed that the disadvantage of the Au catalyst in terms of the higher noble metal mass required for complete CO conversion is offset by the advantage of a lower reverse water gas shift activity of the Au catalyst at 80°C compared with the Pt catalyst at 200°C (43). This advantage becomes particularly critical for CO removal at very low space velocities which cannot be avoided in the case of the load-following requirements for vehicle applications.

The predicted performance of the Au/$\alpha$-$Fe_2O_3$ catalyst in a plug-flow reactor can also be compared with the only other selective CO oxidation study on low-temperature Au catalysts (Au/$MnO_x$) available in the literature (13) [briefly reviewed in Refs. (19, 26)]. There it was shown that 100% conversion of 1 kPa CO with 1 kPa $O_2$ (i.e., $\lambda = 2$) in hydrogen (at atmospheric pressure) could be attained at 50°C. Above this temperature the reaction was oxygen-limited, yielding ~95% conversion at 80°C and ~85% at 120°C. This is consistent with the temperature-dependent loss of selectivity observed in our study. Consequently, higher temperatures require higher $\lambda$ values to completely oxidize CO. Based on our differential flow data we would calculate an oxygen-limited conversion of ~99% for the oxidation of 1 kPa CO with 1 kPa $O_2$ (75 kPa $H_2$, 23 kPa $N_2$) at 80°C and, indeed, we could show that under these conditions CO could be completely oxidized (to below 5 volume-ppm) at a slightly higher $O_2$ partial pressure of 1.15 kPa (43). Therefore, the achievable $O_2$-limited CO conversion of our Au/$\alpha$-$Fe_2O_3$ catalyst is in good agreement with the above selective CO oxidation data for a $MnO_x$-supported Au catalyst. This close agreement between $MnO_x$ and $\alpha$-$Fe_2O_3$-supported Au catalysts clearly points toward a similar $p_{CO}$ dependence of selectivity for both catalysts and to a similar mechanism for the simultaneous oxidation of $H_2$ and CO.

## 5. CONCLUSIONS

We have demonstrated that due to its high activity and selectivity Au/$\alpha$-$Fe_2O_3$ is a very attractive catalyst for selective CO oxidation in fuel cell applications. In simulated reformer gas and at 80°C the kinetics of selective CO oxidation on Au/$\alpha$-$Fe_2O_3$ can be expressed by a simple power-law functionality over wide ranges of CO partial pressures (0.025–1.5 kPa) and $\lambda$ values (0.5–20). The reaction orders with respect to $p_{CO}$ ($\alpha_{CO}$) and $p_{O_2}$ ($\alpha_{O_2}$) were 0.55 and 0.27, respectively. The apparent activation energy for CO oxidation was determined to 31 kJ/mol. The reaction order $\alpha_{CO}$ is strongly temperature dependent, due to the weak adsorption of CO on the gold particles.

The selectivity is independent of $p_{O_2}$ and $\lambda$ and is a function only of the CO partial pressure at constant temperature, decreasing with diminishing $p_{CO}$. The reaction rates of CO and $H_2$ oxidation are not interrelated, which in conjunction with the higher apparent activation energy for $H_2$ oxidation (50 kJ/mol, see Fig. 3a) leads to a loss of selectivity with increasing temperature. Furthermore, the observed selectivity is entirely due to the direct oxidation reactions of both CO and $H_2$ and is not influenced by the water gas shift reaction in our differential flow experiments.

A quantitative comparison of the PROX reaction characteristics over Au/$\alpha$-$Fe_2O_3$ with Pt/$\gamma$-$Al_2O_3$ has shown that the gold catalyst seems to be a superior catalyst for this process, both due to its high activity at the considerably lower temperature of 80°C and to the lower excess oxygen required for a 99% conversion of 1.5% CO in simulated reformer gas.

## ACKNOWLEDGMENTS

This work was supported by the Stiftung Energieforschung Baden-Württemberg (Grant A00008295). We gratefully acknowledge V. Plzak and B. Rohland (Zentrum für Sonnenenergie- und Wasserstoff-Forschung, Ulm) for the catalyst preparation.

## REFERENCES

1. Mann, R. F., Amphlett, J. C., and Peppley, B. A., *Frontiers Sci. Ser.* **7**, 613 (1993).
2. Dönitz, W., Gutmann, G., and Urban, P., *in* "Proceedings of the Second International Symposium on New Materials for Fuel Cell and Modern Battery Systems" (O. Savadogo and P. R. Roberge, Eds.), pp. 14–26. Ecole Polytechnique de Montréal, Montréal, 1997.
3. Murray, H. S., *in* "Fuel Cell," 1985 Fuel Cell Seminar, Book of Abstracts, sponsored by the National Fuel Cell Coordinating Group, Tuscon, AZ, May 1985, p. 129.
4. Kumar, R., and Ahmed, S., *in* "Proceedings of the First International Symposium on New Materials for Fuel Cell Systems" (O. Savadogo, P. R. Roberge, and T. N. Veziroglu, Eds.), pp. 224–238. Ecole Polytechnique de Montréal, Montréal, 1995.
5. Oetjen, H.-F., Schmidt, V. M., Stimming, U., and Trila, F., *J. Electrochem. Soc.* **143**, 3838 (1996).

6. Colsman, G., *in* "Verfahrenstechnische Optimierung der Brenngaserzeugung für Brennstoffzellen in Kraftfahrzeugen," Ph.D. dissertation, RWTH Aachen, 1995.
7. Kahlich, M. J., Gasteiger, H. A., and Behm, R. J., *J. Catal.* **171**, 39 (1997).
8. Cohn, J. G. E., U.S. Patent 3,216,782, Nov. 9, 1965.
9. Bonacci, J. C., Otchy, T. G., and Ackerman, T., U.S. Patent 4,238,468, Dec. 9, 1980.
10. Oh, S. H., and Sinkevitch, R. M., *J. Catal.* **142**, 254 (1993).
11. Plog, C., Maunz, W., Stengel, T., and Andorf, R., European Patent 0,650,922 Al, May 3, 1995.
12. Watanabe, M., Uchida, H., Igarashi, H., and Suzuki, M., *Chem. Lett.*, 21 (1995).
13. Torres Sanchez, R. M., Ueda, A., Tanaka, K., and Haruta, M., *J. Catal.* **168**, 125 (1997).
14. Stephan, J. J., and Ponec, V., *J. Catal.* **42**, 1 (1976).
15. Haruta, M., *Catal. Today* **36**, 153 (1997).
16. Outka, K. A., and Madix, R. J., *Surf. Sci.* **179**, 351 (1987).
17. Sault, A. G., Madix, R. J., and Campbell, C. T., *Surf. Sci.* **169**, 347 (1986).
18. Schwank, J., *Gold Bull.* **16**, 103 (1983).
19. Haruta, M., *Catal. Surv. Jpn.* **1**, 61 (1997).
20. Haruta, M., Kobayashi, T., Sano, H., and Yamada, N., *Chem. Lett.*, 405 (1987).
21. Haruta, M., Kageyama, H., Kamijo, N., Kobayashi, T., and Delannay, F., *in* "Successful Design of Catalysts" (T. Inui, Ed.), p. 33. Elsevier, Amsterdam, 1988.
22. Haruta, M., Yamada, N., Kobayashi, T., and Iijima, S., *J. Catal.* **115**, 301 (1989).
23. Tsubota, S., Yamada, N., Haruta, M., Kobayashi, T., and Nakahara, Y., *Chem. Express* **5**(6), 349 (1990).
24. Haruta, M., Tsubota, S., Kobayashi, T., Kageyama, H., Genet, M. J., and Delmon, B., *J. Catal.* **144**, 175 (1993).
25. Tsubota, S., Cunningham, D., Bando, Y., and Haruta, M., *in* "New Aspects of Spillover Effect in Catalysis" (T. Inui, Ed.), p. 325. Elsevier, Amsterdam, 1993.
26. Haruta, M., Ueda, A., Tsubota, S., and Torres Sanchez, R. M., *Catal. Today* **29**, 443 (1996).
27. Okumura, M., Tanaka, K., Ueda, A., and Haruta, M., *Solid State Ionics* **95**, 143 (1997).
28. Bamwenda, G. R., Tsubota, S., Nakamura, T., and Haruta, M., *Catal. Lett.* **44**, 83 (1997).
29. Gardner, S. D., Hoflund, G. B., Upchurch, B. T., Schryer, D. R., Kielin, E. J., and Schryer, J., *J. Catal.* **129**, 114 (1991).
30. Hoflund, G. B., Gardner, S. D., Schryer, D. R., Upchurch, B. T., and Kielin, E. J., *Appl. Catal. B Environ.* **6**, 117 (1995).
31. Gardner, S. D., Hoflund, G. B., Schryer, D. R., Schryer, J., Upchurch, B. T., and Kielin, E. J., *Langmuir* **7**, 2135 (1991).
32. Lin, S. D., Bollinger, M., and Vannice, M. A., *Catal. Lett.* **17**, 245 (1993).
33. Kang, Y.-M., and Wan, B.-Z., *Catal. Today* **35**, 379 (1997).
34. Epling, W., Hoflund, G. B., and Weaver, J. F., *J. Phys. Chem.* **100**, 9929 (1996).
35. Knell, A., Barnickel, P., Baiker, A., and Wokaun, A., *J. Catal.* **137**, 306 (1992).
36. Yuan, Y., Asakura, K., Wan, H., Tsai, K., and Iwasawa, Y., *Catal. Lett.* **42**, 15 (1996).
37. Yuan, Y., Kozlova, P., Asakura, K., Wan, H., Tsai, K., and Iwasawa, Y., *J. Catal.* **170**, 191 (1997).
38. Bollinger, M. A., and Vannice, M. A., *Appl. Catal. B Environ.* **8**, 417 (1996).
39. Tanielyan, S. K., and Augustine, R. L., *Appl. Catal. A Gen.* **85**, 73 (1992).
40. Cant, N. W., and Ossipoff, N. J., *Catal. Today* **36**, 125 (1997).
41. Badyal, J. P. S., *in* "The Chemical Physics of Solid Surfaces" (D. A. King and D. P. Woodruff, Eds.), Vol. 6. Elsevier, Amsterdam 1993.
42. Levenspiel, O., "Chemical Reaction Engineering," Wiley, New York, 1972.
43. Kahlich, M. J., Gasteiger, H. A., and Behm, R. J., *J. New Mat. Electrochem. Systems* **1**, 39 (1998).
44. Newsome, D. S., *Catal. Rev. Sci. Eng.* **21**, 275 (1980).
45. Sakurai, H., Ueda, A., Kobayashi, T., and Haruta, M., *Chem. Commun.*, 271 (1997).
46. Kahlich, M., Schubert, M. M., Hüttner, M., Noeske, M., Gasteiger, H. A., and Behm, R. J., *in* "Proceedings of the 2nd International Symposium on New Materials for Fuel Cell and Modern Battery Systems" (O. Savadogo, Ed.), pp. 642–653. Ecole Polytechnique de Montréal, Montréal, 1997.
47. Schubert, M. M., Gasteiger, H. A., and Behm, R. J., unpublished results.
48. Li, Y.-E., Boecker, D., and Gonzales, R. D., *J. Catal.* **110**, 319 (1988).
49. Engel, T., and Ertl, G., *Adv. Catal.* **28**, 1 (1979).
50. Thiel, P. A., Behm, R. J., Norton, P. R., and Ertl, G., *J. Chem. Phys.* **78**, 7448 (1983).
51. Seebauer, E. G., Kong, A. C. F., and Schmidt, L. D., *Surf. Sci.* **176**, 134 (1986).
52. Wartnaby, C. E., Stuck, A., Yeo, Y. Y., and King, D. A., *J. Phys. Chem.* **100**, 12483 (1996).
53. McElhiney, G., and Pritchard, J., *Surf. Sci.* **60**, 397 (1976).
54. Kottke, M. L., Greenler, R. G., and Tompkins, H. G., *Surf. Sci.* **32**, 231 (1972).
55. Ruggiero, C., and Hollins, P., *J. Chem. Soc. Faraday Trans.* **92**, 4829 (1996).
56. Boccuzzi, F., Chiorino, A., Tsubota, S., and Haruta, M., *J. Phys. Chem.* **100**, 3625 (1996).
57. Cant, N. W., and Fredrickson, P. W., *J. Catal.* **37**, 531 (1975).